Helium and Hydrogen Adsorbed on Spheres and Cylinders

E. S. Hernández & L. Szybisz

Journal of Low Temperature Physics

ISSN 0022-2291

J Low Temp Phys
DOI 10.1007/s10909-014-1164-y

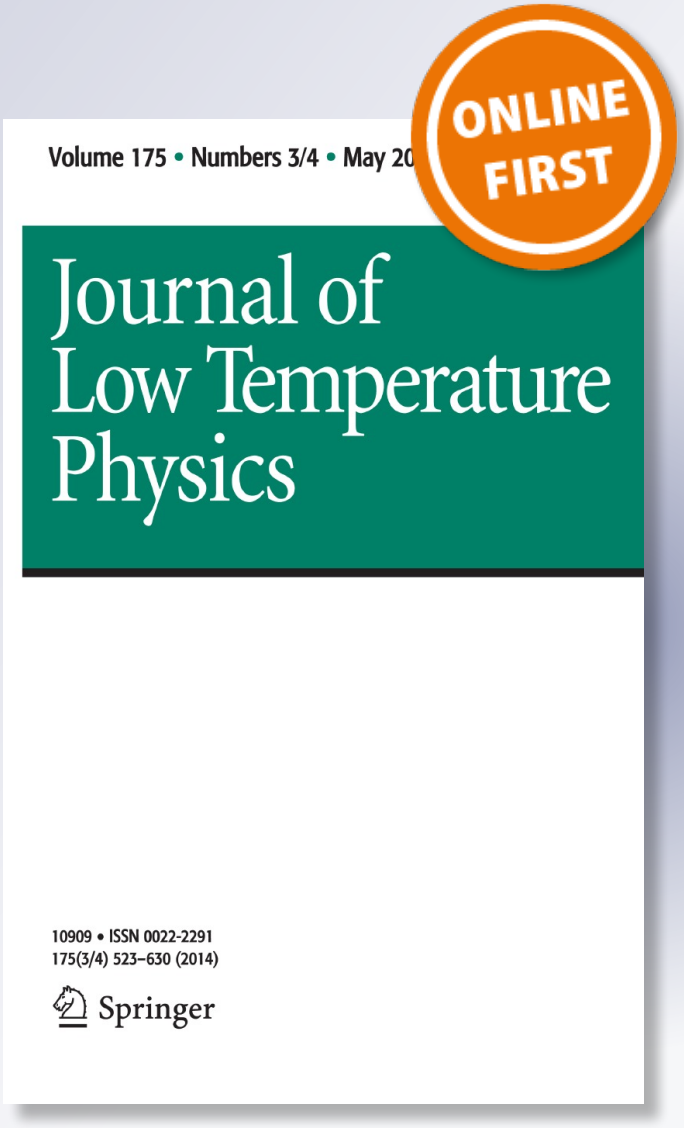

Springer

J Low Temp Phys
DOI 10.1007/s10909-014-1164-y

Helium and Hydrogen Adsorbed on Spheres and Cylinders

E. S. Hernández · L. Szybisz

Received: 10 December 2013 / Accepted: 10 March 2014

Abstract We examine the metastable and unstable regimes of condensation of superfluid helium and parahydrogen on spheres and cylinders at finite temperatures, employing finite range density functionals. The goal is to compare calculations of sizes and spreads of films at the onset of metastability and of instability with the predictions of a simple phenomenological model that contemplates the curvature of the substrate. We have focused on two cases, helium on nanospheres and nanocylinders of different materials, and hydrogen on fullerenes. We are able to locate the onset of metastability and of spinodal instability in the adsorption isotherms of every sample and to extract the width of the condensed fluid. It is shown that the predictions of the so-called simple model agree surprisingly well with the more elaborate calculations.

Keywords Curved substrates · Adsorption · Instabilities · Film spread · Density functional

1 Introduction

Since the discovery of wetting transitions [1], that take place at a temperature T_W above which a liquid (l) phase uniformly fills the gap between a solid (s) wall and a

E. S. Hernández (✉) · L. Szybisz
Departamento de Física/IFIBA, Facultad de Ciencias Exactas y Naturales, Universidad de Buenos Aires, Buenos Aires, Argentina
e-mail: shernand@df.uba.ar

L. Szybisz
e-mail: szybisz@tandar.cnea.gov.ar

E. S. Hernández
Instituto de Física de Buenos Aires, Buenos Aires, Argentina

L. Szybisz
Comisión Nacional de Energía Atómica, Buenos Aires, Argentina

Published online: 29 March 2014

vapor (v), the onset of wetting is expressed in terms of the vanishing of the spreading power $S = \sigma_{sv} - (\sigma_{sl} + \sigma_{lv})$ that gives the balance among the surface tensions σ_{ij} at each interface. While originally most of the experimental and theoretical work on these transitions placed the focus on flat substrates, the observation of wetting of silica spheres immersed in a binary liquid mixture [2], as well as the employ of graphite fibers in microbalances to observe adsorption of superfluid helium [3], called attention on the specific features of curved adsorbers. The first insight stems from Antonoff's rule [4], that establishes that for a film of width l on a cylindrical or spherical substrate of radius R, the surface energy balance at the onset of wetting corresponds instead to the vanishing of the modified spreading power

$$S(l) = \sigma_{sv} - \left[\sigma_{sl} + \sigma_{lv}\left(\frac{R+l}{R}\right)^{\tau}\right] \tag{1}$$

with $\tau = 1$ for cylinders and 2 for spheres. The extra factor is the ratio between the areas at the lv and the sl interfaces of the film. This relation shows that unbound film growth is prevented for any finite value of the substrate radius. This result was reinforced by theoretical arguments that invoke mean field theory [4], Landau theory [5,6] and interfacial models [5,7–9].

In spite of the limitations of these approaches, that in general do not take into account the modifications of the lv surface tension with the width of the film as pointed out e.g in Ref. [8], specific calculations for adsorption of ^{4}He on spheres [10–13] and cylinders [14] at zero temperature, performed in the frame of finite range density functional theory, demonstrated that the isotherms $\mu(x)$, with μ the chemical potential of the helium atoms and with x the total number of particles condensed on a sphere (N) or particles per unit length on a cylinder (n), exhibit a maximum corresponding to a spinodal instability at a size x_s, where the chemical potential is larger than the bulk value μ_B and its derivative $\left.\frac{d\mu}{dx}\right|_{x_s}$ vanishes. In other words, adsorption films of helium on curved substrates become metastable—with positive derivative—at some film size $x_m < x_s$ such that $\mu(x_m) = \mu_B$, and unstable for values of x higher than x_s, where $d\mu/dx$ is negative. In fact, adsorption of helium and hydrogen on carbon nanotubes and fullerenes has been investigated from various viewpoints along the last decade [15,16] (see as well the reviews in Ref. [17]); moreover, the recent incorporation of density functionals designed to describe the equation of state of bulk helium [18] and hydrogen [19,20] at finite temperatures (FTDF) opened the possibility of investigating various thermodynamic properties of fluid adsorption, as in the case of ^{4}He on nanostructured substrates [21].

The purpose of this work is to take a deeper view of the metastable–unstable regimes of condensation of quantum fluids on spheres and cylinders at FTDF. In fact, as presented in Sect. 1, very simple assumptions that exhibit the macroscopic features of the energetics of an adsorbed film, lead to schematic formulae for the spread of the fluid at the onset of metastability and of instability on such substrates. In Sect. 2, we apply the FTDF of Ref. [18] to compute the one-dimensional density profiles of helium on nanospheres coated with Mg. The reason for this choice is that Mg is a strong adsorber, however milder than carbon in fullerenes [10], which permits a much

more efficient use of long calculation times for the sake of illustrating the regime of interest, with the possibility of confronting the results with the predictions of a simpler phenomenological model. A similar treatment of helium on Mg cylinders is presented in Sect. 3. In Sect. 4 we investigate condensation of hydrogen on fullerenes, with a discussion on the advantages and disadvantages of the FTDF's of Refs. [19] and [20]. Our summary and conclusions are presented in Sect. 6.

2 Simple Model of Fluid Condensation on Spheres and Cylinders

The basis of the so-called simple model for a film on a curved substrate is the mass formula for a finite system with N particles adsorbed on a substrate

$$E = \mu_B N + \sigma A + \int dN\, V_s \tag{2}$$

where E is the total energy, μ_B the bulk chemical potential or energy per particle in the thermodynamic limit, σ the surface tension, A the total area of the film and V_s the substrate adhesive potential. We assume that this expression is valid at all temperatures, with V_s independent of T. For N particles on a sphere with radius R, distributed on an uniform film of width l, the total area that includes both film surfaces is

$$A = 4\pi\,[(R+l)^2 + R^2] \tag{3}$$

and with ρ the density of the homogeneous film, the number of particles is

$$N = \frac{4}{3}\,\pi\,\rho\,[(R+l)^3 - R^3] \tag{4}$$

If we define an average coverage as $\frac{1}{n} = \left.\frac{dA}{dN}\right|_l$ and use the chain rule with l as an intermediate variable, we get

$$\frac{1}{n} = \frac{2}{\rho\,(R+l)} \tag{5}$$

From Eq. (2) we obtain the chemical potential $\mu(N) = \left.\frac{\partial E}{\partial N}\right|_R$ of the finite system as

$$\mu(N) = \mu_B + \frac{\sigma}{n} + V_s \tag{6}$$

and with the help of (5) we can derive the following conditions:

1. At a film thickness l_s corresponding to the maximum of the $\mu(N)$ isotherm at $\frac{d\mu}{dl} = 0$, the relation

$$R + l_s = \sqrt{\frac{2\sigma}{\rho\, V_s'(l_s)}} \tag{7}$$

where the rhs coincides with the capillary length, is a force balance equation. This indicates that the onset of instability takes place when gravity and capillary forces compensate.

2. For the threshold of metastability at a film thickness l_m corresponding to the crossover $\mu = \mu_B$, Eq. (6) gives

$$R + l_m = -\frac{2\sigma}{\rho\, V_s(l_m)} \tag{8}$$

This is an energy balance equation, where the substrate energy compensates the work of capillary forces needed to displace one particle along a distance l_m from the surface of the adsorber at saturation density.

Similar consideration for the case of N particles coating the lateral surface of a cylinder of length L and radius R give

$$R + l_s = \sqrt{\frac{\sigma}{\rho\, V_s'(l_s)}} \tag{9}$$

$$R + l_m = -\frac{\sigma}{\rho\, V_s(l_m)} \tag{10}$$

3 Helium on Mg Spheres

We present some results for the growth of a helium film on a Mg sphere with radius 3 Å, obtained using the FTDF of Ref. [18]. The film growth on such spheres at zero temperature has been discussed in Ref. [11], using the Lennard–Jones (LJ) He–Mg interaction in Table I of Ref. [10]. This same interaction is selected in the present work, where the sphere radius is chosen deliberately small—only slightly above the minimum size at which condensation takes place, as reported in [11]—to secure that the instability takes place within a couple of layers; in fact, we compute isotherms for a few temperatures near zero and look for the maximum as a function of N as illustrated in Fig. 1. For nonvanishing (low) T's the isotherm simply moves slightly downwards as illustrated by the calculation of a few points near the maximum to note the trend, and the maximum-located at $N = 175$ for zero temperature—moves slightly righwards. As seen in this figure, the numerical results for $T = 0.4$ and 0.6 K cannot be distinguished, although they visibly depart from the $T = 0$ data.

The numerical thickness $l_s = R_R - R_L$ is obtained from the density profiles, where R_L and R_R are the left and right edges of the film at half the saturation density ρ_{sat} as shown in Fig. 2. The details appear in Table 1 together with the solution of Eq. (7), where input data for the saturation density are taken from Ref. [18] while those for the surface tension were kindly provided by F. Ancilotto, and $V_s'(l_s)$ is the force at the position R_R. For completeness, Table 1 also shows the corresponding results for the spread of the film at the threshold of metastability, with numerical results for Eq. (8). For this sphere, the width l_m at metastability threshold correspond to a monolayer film with nearly 50 particles and its temperature dependence is not visible in the displayed scale.

For a film of thickness $l_{s,m}$ extending between R_L and R_R, the edge R_L plays the role of the adsorber radius R in Eqs. (7) and (8), so the quantity to be compared with the simple model prediction $R + l_{s,m}$ is the outer edge, R_R. Surprisingly enough, in view of the important shell structure of the film, the simple formula works quite well

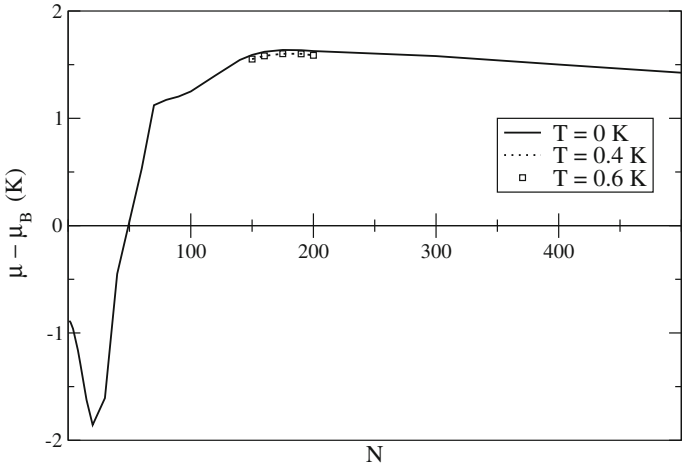

Fig. 1 Chemical potential of helium films on a Mg sphere at zero temperature, as a function of the number of adsorbed atoms

Table 1 Total extension (R_R) and widths $l_{m,s}$ of ^{4} He films on Mg spheres from FTDF calculations together with the simple model predictions

T (K)	R_R (Å) from density profile	$R + l_s$ (Å) from Eq. (7)	R_R (Å) from density profile	$R + l_m$ (Å) from Eq. (8)
0	12.51	12.36	9.33	8.92
0.4	12.49	12.38	9.33	8.96
0.6	12.46	12.39	9.33	8.97

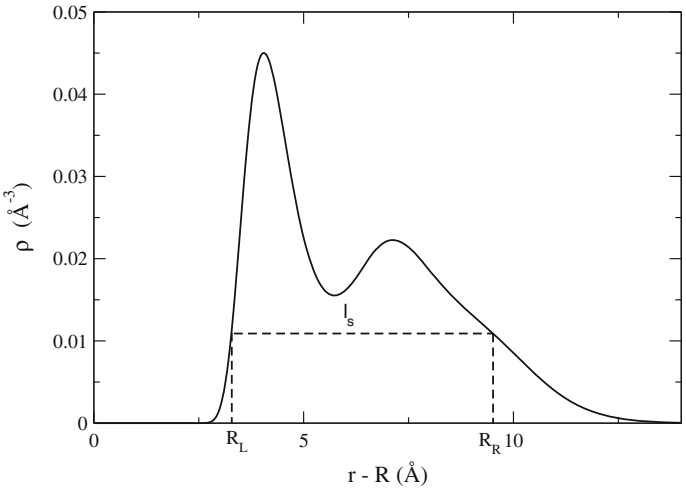

Fig. 2 Density profile of the helium film on a Mg sphere at zero temperature, at the position of the maximum of the isotherm in Fig. 1, as a function of the distance to the sphere's surface

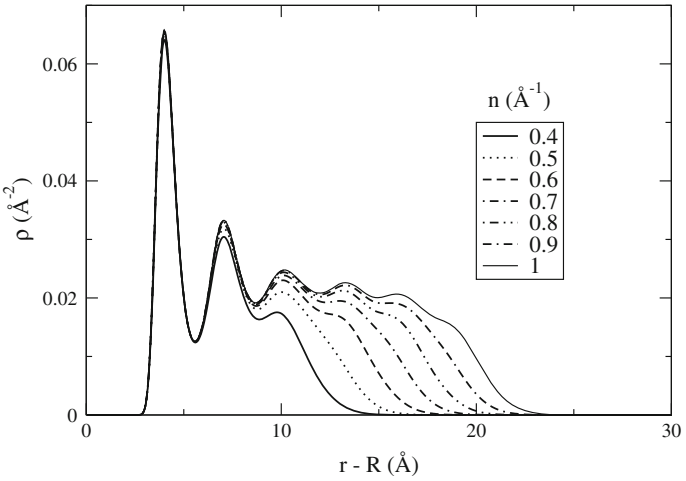

Fig. 3 Density profiles of helium films on a Mg coated cylinder at zero temperature as functions of the distance to the cylinder surface, for various coverages. Note that for coverages higher than around 0.7 Å^{-1} the films are metastable (cf. Fig. 4)

if the proper parameters are introduced, especially for the location of the spinodal instability.

4 Helium on Mg Cylinders

Figure 3 displays density profiles for several coverages $n = N/L$ for a Mg coated cylinder with a radius $R = 7$ Å, computed at $T = 0$, for the same FTDF and He–Mg interaction as in the previous section. These curves are plotted over a wide range of coverages in order to illustrate the succesive layering that takes place even in the metastable regime, $\mu > \mu_B$. For the sake of comparison, Fig. 4 also shows the zero temperature isotherms for helium on carbon nanotubes withr R = 7 Åwith the helium–carbon LJ interaction of Ref. [10], and for helium on the outer surface of an Au cylinder with R = 12 Å as presented in Ref. [14]. The density profiles at the maxima of these isotherms are shown in Fig. 5. The solutions of Eqs. (9) and (10) are displayed in Table 2 together with those obtained from the density profiles.

We note that in this case, the predictions of the simple model underestimate the film thickness by amounts as large as 30 %, both at the threshold of metastability and at the spinodal point, at variance with the case of a small sphere. This is not surprising in view of the pronounced shell structure and the high solid peaks in the first two layers.

5 Hydrogen on Fullerenes

Recently, two FTDF's for molecular parahydrogen have been proposed [19,20]. The major difference between these descriptions lies in the expression for the free energy

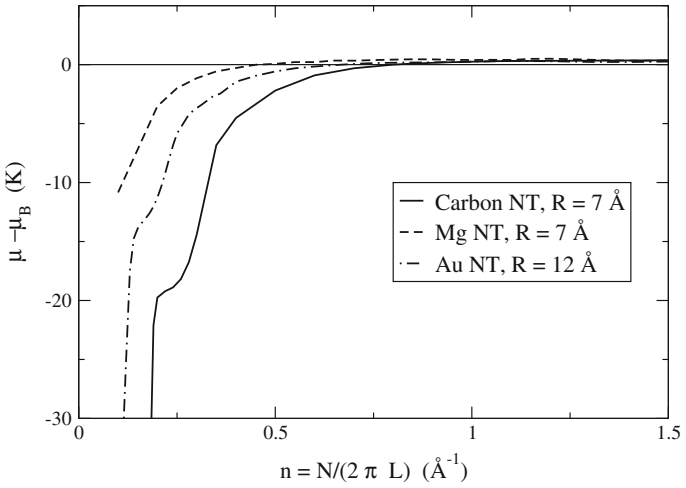

Fig. 4 Zero temperature isotherms for helium on nanotubes of various sizes and materials

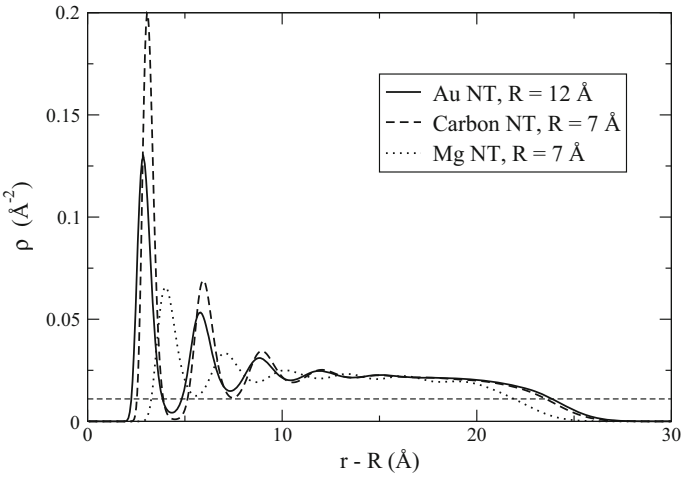

Fig. 5 Density profiles of the films at the maxima of the isotherms in Fig. 4 as functions of the distance to the cylinder surface. The *horizontal line* corresponds to the value $\rho_{sat}/2$

Table 2 Total extension (R_R) and widths $l_{m,s}$ of ^{4}He films on cylinders of different materials and radii together with the simple model predictions.

Substrate	R_R (Å) from density profile	$R + l_s$ (Å) from Eq. (9)	R_R (Å) from density profile	$R + l_m$ (Å) from Eq. (10)
Au, $R = 12$ Å	35.96	26.87	28.19	15.38
C, $R = 7$ Å	30.62	23.05	18.91	16.72
Mg, $R = 7$ Å	28.94	20.94	22.21	15.33

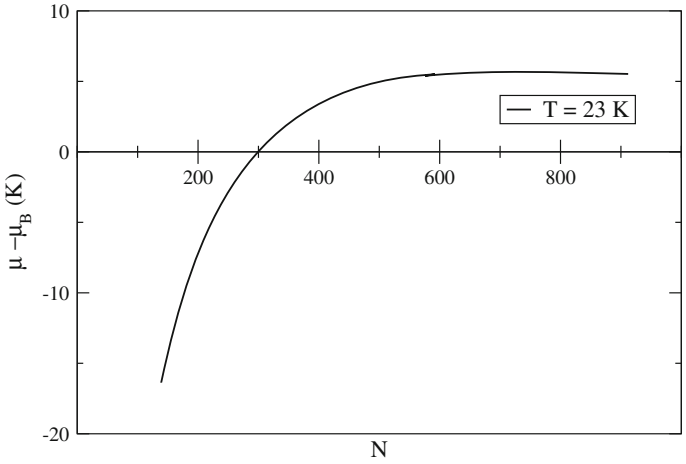

Fig. 6 Chemical potential as a function of the number of hydrogen molecules adsorbed on C_{60} at $T = 23\,\mathrm{K}$

of the noninteracting gas that enters the kernel of the density functional, which in Ref. [19] is that of a classical ideal gas, while in Ref. [20] the philosophy is identical to the case of liquid helium [18] where the ideal system is a free Bose gas. A detailed account of the adjustment of parameters and predictions of these two FTDF's will be given in a nextcoming work; for our current purpose, we have verified that to a satisfactory extent, the computed density profiles and isotherms are not sensitive to the input choice.

We have performed calculations for molecular hydrogen adsorbed on a C_{60} fullerene at various temperatures. A typical adsorption isotherm computed with the FTDF in Ref. [20], using the LJ hydrogen–carbon interaction given in [10], is presented in Fig. 6, where the chemical potential of the H_2 molecules is shown as a function of particle number for $T = 23\,\mathrm{K}$. This calculation has been done with a high resolution in the variable N, as seen in Fig. 7, where the details near the maximum at $N = 720$ are displayed. The choice of such a high resolution also inhibits computations for numbers of molecules below $N = 100$, which, moreeover, lie far away from the region of metastability.

The density profile at the maximum is shown in Fig. 8 employing both FTDF's, without any visible departure. The evolution of the isotherm with temperature in the vicinity of the peak is illustrated in Fig. 9, where the simpler FTDF of Ref. [19] has been employed to benefit from numerical fastness; the predictions of the two FTDF's employed can be observed for $T = 23\,\mathrm{K}$, showing that no substantial difference in trends appears for the system under consideration.

The sizes and spreads of the films at the maxima in Fig. 9 are shown in Table 3, showing that once again, the predictions of the simple model are remarkably good. As an illustration, the density profile at the spinodal instability at $T = 24\,\mathrm{K}$ is plotted in Fig. 10, exhibiting the important solid peaks incorporated into the size and spread of the film.

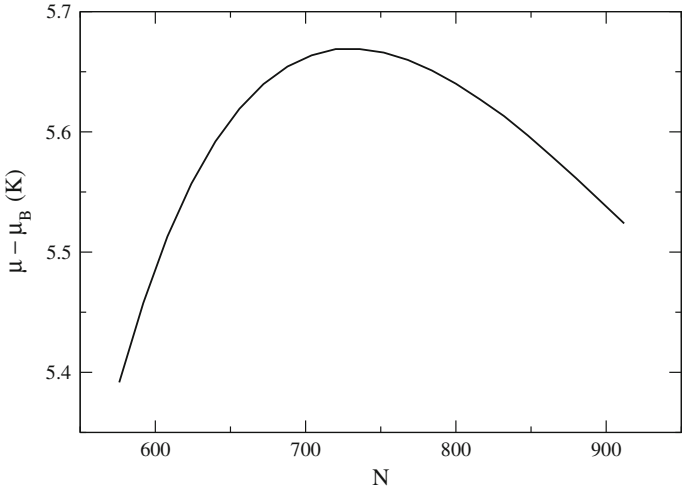

Fig. 7 Same as Fig. 6 near the maximum of the chemical potential

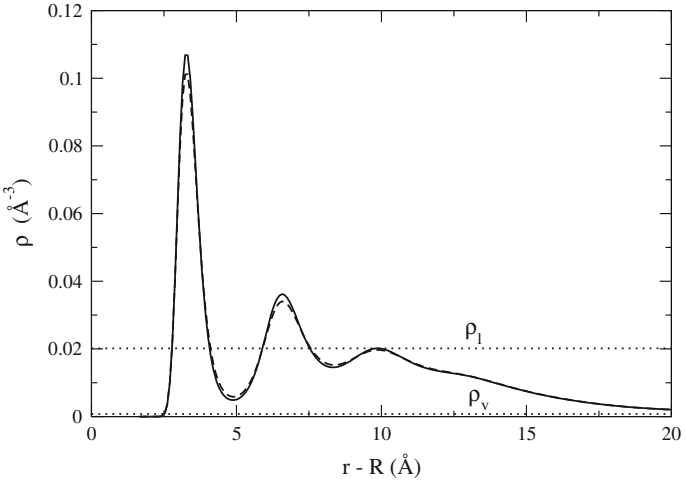

Fig. 8 Density profile as a function of the distance to the fullerene's center. The *solid* (*dashed*) *line* were respectively obtained with the FTDF's in Refs. [20] and [19]

6 Summary

In this work we have considered the metastable and unstable regimes of condensation of superfluid helium and parahydrogen on spheres and cylinders at FTDF. The goal has been to compare FTDF calculations of sizes and spreads of films at the onset of metastability and of instability with the predictions of a simple phenomenological model. We have focused on two sample situations, designed to take advantage of the available FTDF's; helium on spheres and cylinders and hydrogen on fullerenes. The choices are made in order to extract characteristics of the adsorption process

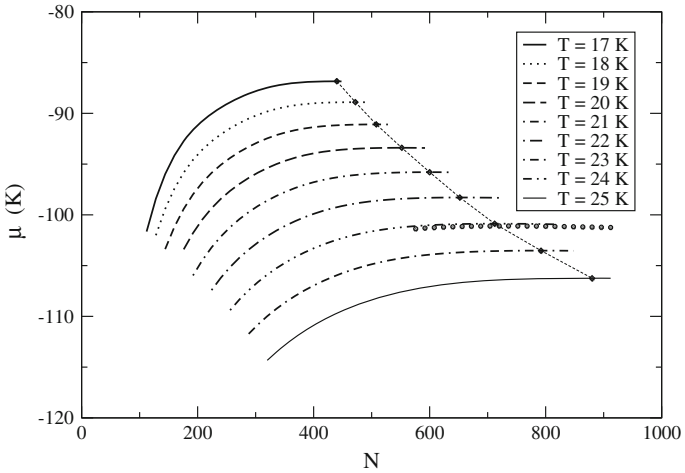

Fig. 9 Reduced chemical potential as a function of the number of particles for temperatures from $T = 17$ (*top*) to 25 K (*bottom*). The *lines* stand for results evaluated with the FTDF of Ref. [19], while the *small circles* are data obtained with the FTDF in Ref. [20]. The *dashed line* joints the location of the maxima

Table 3 Film's widths for H_2 on C_{60} spheres and simple model predictions

T (K)	R_R (Å) from density profile	$R + l_s$ (Å) from Eq. (7)	R_R (Å) from density profile	$R + l_m$ (Å) from Eq. (8)
17	15.20	13.57	10.67	9.88
18	15.46	13.70	10.72	9.97
19	15.76	13.84	10.80	10.06
20	16.17	13.99	10.88	10.16
21	16.57	14.15	10.98	10.27
22	16.93	14.33	11.09	10.39
23	17.34	14.53	11.20	10.53
24	17.93	14.76	11.30	10.68
25	18.59	15.01	11.50	10.86

at the lowest possible computational cost; this criterion led to the selection of small Mg spheres, carbon nanotubes, and Mg and Au cylinders wetted by helium, and of C_{60} fullerenes coated with parahydrogen. In the latter case, a thoughtful comparison between predictions of two FTDF's [19,20] allowed us to select the simplest version of Ref. [19] for the computationally intensive calculations.

It is important to mention that a study of adsorption of parahydrogen on C_n fullerenes, based on quantum Monte Carlo techniques, was carried by Turnbull and Boninsegni [22]. To the best of our knowledge this is the first calculation of this sort, with the focus on the relevance of corrugation on the energy per particle as a function of the number of adsorbed molecules for different fullerene sizes. In this work, a single stable adsorption layer is encountered; likely due to the characteristics of the method, the calculations stop far below the bulk chemical potential, so that

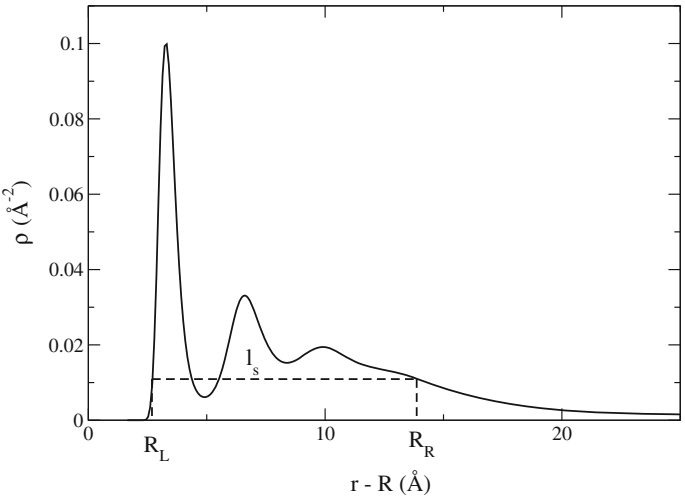

Fig. 10 Density profile at $T = 24\,\mathrm{K}$ as a function of the distance to the fullerene's surface. The *solid line* was obtained with the DF in Ref. [19] for $N = 792$. The distance ℓ_s along the *dashed line* between R_R and R_L is the width of the film

the metastability regime is not reached. However, at the largest numbers of adsorbed molecules, the effects of corrugation are remarkably smoothed away. This results give further support to the application of FTDF to systems with chemical potential close to the saturation value, as done in the present work.

Generally speaking, the various instabilities appearing in an isotherm $\mu(N)$ (spheres) or $\mu(n)$ (cylinders) can be associated to the layering process along the adsorption path. The maxima of $\mu(n)$ are critical points where capillary forces balance the gravity exerted by the substrate; for sligthly thicker films the former are not sufficient to hold the film together, and any physical film should undergo phase separation. When spinodal instabilities of this sort take place along the layering process, the system stabilizes by promoting particles to a new layer. In this respect, the instability contemplated in this work is not different from any layering instability observed in an adsorption isotherm.

However, when the chemical potential is higher than the saturation value the system is no longer bound with respect to the bulk liquid, and the fluid sample becomes thermodynamically metastable. This is intrinsic to curved substrates; the simple model in Sect. 2 shows that the identity $\mu = \mu_b$ can take place at a finite value of the width l only if the coverage—in other words, if the total area of the film and/or the number of condensed particles—depends on the thickness. There is a smooth evolution from metastability to spinodal instability, and the latter persists up to the thermodynamic limit, $l \longrightarrow \infty$. In these cases, the continuity of the calculated isotherm is an artifact of the FTDF method, that obtains the chemical potential for any fixed amount of material.

Finally, it is worthwhile noting the rather reliable performance of the so-called simple model, that proves to be able to yield gross features of the regimes of interest within the correct scales, in spite of the sizeable shell structure of the condensed fluids.

The criterion to compute the film size within FTDF—namely, setting the film edges at half the saturation density—might seem arbitrary; however, we note that this is the standard definition of the size of finite systems, such as atomic nuclei, drops, and clusters of any kind. It is clear that any other choice of the film size would yield different comparisons with the simple model.

Acknowledgments The authors are pleased to acknowledge fruitful conversations with M. Cole on the physics of the phenomenological approximation, and interesting discussions with F. Ancilotto during the first stages of the calculations. This work was performed with partial support from grants PIP 0546 from CONICET, UBACYT 01/K156 from University of Buenos Aires and PICT 2011/1217 from ANPCYT, Argentina.

References

1. J.W. Cahn, J. Chem. Phys. **66**, 3667 (1977)
2. D. Beysens, D. Estève, Phys. Rev. Lett. **54**, 2123 (1985)
3. P. Taborek, L. Senator, Phys. Rev. Lett. **57**, 218 (1986)
4. R. Holyst, A. Poniewierski, Phys. Rev. B **36**, 5628 (1987)
5. M. Gelfand, E. Lipowsky, Phys. Rev. B **36**, 8725 (1987)
6. P.J. Upton, J.O. Indekeu, J.M. Yeomans, Phys. Rev. B **40**, 666 (1989)
7. T. Bieker, S. Dietrich, Phys. A **252**, 85 (1998)
8. R. Evans, R. Roth, P. Bryk, Eur. Lett. **62**, 815 (2003)
9. A.O. Parry, C. Rascón, L. Morgan, J. Chem. Phys. **124**, 151101 (2006)
10. E.S. Hernández, M.W. Cole, M. Boninsegni, Phys. Rev. B **68**, 1254181 (2003)
11. E.S. Hernández, M.W. Cole, M. Boninsegni, J. Low Temp. Phys. **134**, 309 (2004)
12. L. Szybisz, I. Urrutia, J. Low Temp. Phys. **134**, 1079 (2004)
13. E.S. Hernández, J. Low Temp. Phys. **138**, 241 (2005)
14. E.S. Hernández, J. Low Temp. Phys. **137**, 89 (2004)
15. R.B. Hallock, Y.H. Kahng, J. Low Temp. Phys. **134**, 21 (2004)
16. M.C. Gordillo, J. Boronat, Phys. Rev. B **86**, 165409 (2012)
17. E.J. Bottani, J.M.D. Tascón (eds.), *Adsorption by Carbons: Novel Carbon Adsorbents* (Elsevier, Amsterdam, 2008)
18. F. Ancilotto, F. Faccin, F. Toigo, Phys. Rev. B **62**, 17035 (2000)
19. M.S. Pettersen, J. Low Temp. Phys. **157**, 137 (2009)
20. J. Navarro, F. Ancilotto, M. Barranco, M. Pi, J. Phys. Chem. A **115**, 6910 (2011)
21. F. Ancilotto, M. Barranco, E.S. Hernández, A. Hernando, M. Pi, Phys. Rev. B **79**, 1045141 (2009)
22. J.D. Turnbull, M. Boninsegni, Phys. Rev. B **71**, 205421 (2005)